Article:
Abdul-Wahab, SA, Al-Dhamri, H, Ram, G et al. (2020) The use of oil-based mud cuttings as an alternative raw material to produce high sulfate-resistant oil well cement. Journal of Cleaner Production, 269. 122207. ISSN: 0959-6526

https://doi.org/10.1016/j.jclepro.2020.122207

8959 Words

The use of oil-based mud cuttings as an alternative raw material to produce high sulfate-resistant oil well cement

Sabah A. Abdul-Wahab [a, *], Hilal Al-Dhamri [a, b, c], Ganesh Ram [b], Leon Black [c]

[a] *Department of Mechanical and Industrial Engineering, Sultan Qaboos University, Muscat, Sultanate of Oman*
[b] *Oman Cement Company S.A.O.G, Muscat, Sultanate of Oman*
[c] *School of Civil Engineering, University of Leeds, United Kingdom*

A B S T R A C T

Oil-based mud (OBM) is used during the oil well drilling processes to cool drilling pits and remove the cuttings. As a result of these processes, the oil-based mud (OBM) cuttings are produced. The composition of the OBM cuttings depends on the geological conditions of the boreholes and the OBM used during the drilling operation. In this study, the OBM cuttings were used as an alternative material to produce a special cement known as oil-well cement (OWC). Raw meal mixtures were prepared with various percentages of OBM cuttings (5, 11, 13, 15, 18, and 20%). Then they were sintered up to a temperature of 1450 ºC, and the resulting cement clinker was ground to produce highly sulfate resistant OWC. The burnability of the raw meal was studied to explore the effect of OBM cuttings on raw meal behavior during the clinkerization process. The results of the study indicated a decrease in the decarbonation temperature and an increase in the rate of clinkerization as the OBM cuttings increased. The produced cement was tested per American Petroleum Institute's testing procedure for OWC. Also, the cement hydration for 2, 7 and 28 days was carried out to study the behavior of the produced OWC.

Keywords:
Thermal Analysis
Mineralizers
Burnability
Decarbonation
Rosin-Rammler Distribution
Phase Formation

*Corresponding author.
E-mail address: sabah1@squ.edu.om (Sabah A. Abdul-Wahab).

Abbreviations and acronyms

AR	Alumina ratio
Bc	Bearden consistency scale
C_3S	Tricalcium silicate
C_2S	Dicalcium silicate
C_3A	Tricalcium aluminate
C_4AF	Tetra calcium alumino ferrite
DSC	Differential scanning calorimetry
FF	Free fluid test
HPHT	High-pressure high-temperature consistometer
kcps	kilo counts per second
LSF	Lime saturation factor
OBM	Oil-based mud
OCC	Oman Cement Company
OWC	Oil well cement
PSD	Particle size distribution
RRD	Rosin-Rammler Distribution
SD	Slurry density
SEM	scanning electron microscopy
SR	Silica ratio
TGA	Thermogravimetric analysis
w/c	water-to-cement ratio
XRD	X-ray diffractometry

1. Introduction

Amongst the world's major industries, the petroleum and gas industry plays a vital role in fulfilling global energy demand, with oil and gas providing, respectively, for 31% and 23% of the total global energy supply in 2018 (The International Energy Agency, 2019). The Sultanate of Oman contributed around 1% of the world's total oil production for 2018, producing on average 978,000 barrels per day with a growth of 0.8% from 2017 (BP Statistical Review of World Energy, 2019). The production of oil and gas results in the co-production of waste materials, some of which are environmentally hazardous. The predominant waste is drill cuttings, comprising soil cuttings mixed with oil-based drilling fluids, generally referred to as oil-based (OBM) cuttings (Siddique et al., 2017). These OBM cuttings are considered potentially hazardous for the surrounding environment due to the presence of hydrocarbons and their chemical composition (Davies et al., 1984). The inorganic chemical composition of these OBM cuttings is predominantly defined by the geology around the well (Abdul-Wahab et al., 2016) while the cuttings may also contain 6-17 wt.% of diesel oil, which adheres to the cuttings (Dow et al., 1990). Discharge-related pollutants, like hydrocarbons and heavy metals within the cuttings, may have both acute and chronic toxicological effects through post-sedimentary migration of contaminants within the sediment or leakage into the areas surrounding the drilling site (Allers et al., 2013). Waste cuttings can also spread by air, although this type of dissemination is greatly influenced by the cuttings' particle size, which can range from 2 to 275 microns (Al-Dhamri et al., 2019a).

In Oman, most oil exploration sites are on top of limestone deposits (Al-Dhamri et al., 2019b). The OBM cuttings from Oman's PDO sites located at Qarn-Alam and Fahud contain calcium as calcium carbonate, which is the main raw material for cement production. So, along with the calorific content of the oil and drilling fluids, this calcium-rich waste material could be utilized as a raw material in cement production. Furthermore, as the cement manufacturing

process involves a high-temperature pyro-process, the addition of hazardous industrial wastes like OBM cuttings is a viable and safe way to dispose of such material (Van Oss and Padovani, 2002). This study focuses on the utilization of these calcium-rich OBM cuttings generated as waste during oil well drilling as a raw material for oil well cement (OWC) clinker production. This adoption of a circular economy approach, with an associated reduction in allocated CO_2 emissions, is of great value to a cement industry responsible for 7% of global greenhouse gas emissions.

Abdul-Wahab et al. (2016) determined a fall in allocated CO_2 emissions during the calcination process in clinker manufacture when using OBM cutting waste as a raw material. Due to its high raw material and fossil fuel consumption, the cement industry is keen to explore the use of industrial by-products as replacements. As part of this drive to circularity, developing economically viable more environmentally-friendly products, the cement industry has undertaken numerous studies into the replacement of raw materials with wastes and industrial by-products (Chatterjee, 2018). Such studies have provided significant opportunities to utilize large quantities of such industrial waste systematically and could reduce the cost of cement production (Barthel et al., 2016), plus reduce abiotic depletion and allocated CO_2 emissions.

OBM cuttings used as a partial substitution for shale to produce sintered bricks. The physico-mechanical properties of OBM cuttings after sintering at 950–1050 ^{o}C were examined by Li et al. (2011), and leaching of heavy metals was found to be within allowable limits. The study focused on replacing cement clinker with between 5–20% OBM cutting waste, with X-ray diffractometry (XRD) and scanning electron microscopy (SEM) revealing densification as the sintering temperature increased.

Much as with fly ash and silica fume, treated drill cuttings have also been investigated as cement replacements. When looking at incorporation into concrete, a 10% reduction in strength was observed when 5% of the cement was replaced by dried drill cuttings. However,

98 the compressive strength was reduced by 20% when 10%, 15% and 20% of the cement was
99 replaced. When examining the effect of fly ash and silica fume additives on concrete samples
100 made with drill cuttings, a significant impact on the compressive strength of the cement sample
101 was found (Mostavi et al., 2015). This suggests the need for a more effective route for utilizing
102 OBM drill cuttings.

103 A study on the use of treated OBM cuttings, namely modified drilling waste materials
104 (MDWMs), as base course material in road construction evaluated MDWMs constituting 3%
105 of a cement mixture. The results showed a good performance that satisfied the requirements
106 for a class-M base due to high pH, low plasticity, and the addition of clay sand material (Shon
107 et al., 2016). Al-Futaisi et al. (2007) researched tank bottom oily sludge waste when used as a
108 fuel supplement, in solidification, and as road material, finding that the carbon content seemed
109 comparable with other fuels like bituminous coal, sewage sludge (SS), and meat and bone meal
110 (MBM). They also assessed the toxicity characteristics and leaching behavior of a solidified
111 sludge mixture and in road applications. The lack of the leachability of heavy metals from the
112 oily sludge mixture suggested that sludge applications should not be considered hazardous. A
113 technical feasibility study showed that drill cuttings dried, ground, pelletized and sintered at
114 1160–1190 ºC could be used as aggregate in lightweight concrete (Ayati et al., 2019). The
115 lightweight aggregate had a particle density of 1.29 g/cm^3, water absorption of 3.6%, and
116 compressive strength of 4.4 MPa. The results pointed to an efficient option for reusing drilling
117 waste.

118 However, all the research mentioned above used OBM wastes to produce low-energy,
119 low-value products, like aggregates. This doesn't necessarily ensure efficient circularity. As
120 mentioned above, OBM cuttings are a source of calcium, with a calorific value. As such, they
121 may be appropriate to produce Portland cements, including oil well cements. Oil well cements
122 are Portland cements with modified compositions and performance to meet the demanding

conditions within an oil well. Various oil well cements are manufactured worldwide according to customer needs as per local and international standards. In petroleum drilling operations, special oil well cements have been standardized by the American Petroleum Institute (API) for different cementing applications (API Spec 10A, 2019), including sealing of annulus after a casing string has been run in a wellbore, sealing a lost circulation zone, and sealing an area in an oil well with a reduction or absence of flow (Nelson and Guillot, 2006). The conditions inside an oil well rig significantly differ from surface conditions during construction operations so, in response, well cements are developed as special cements (Zhang et al., 2010).

This study exploits the close geographical proximity of OBM cuttings and the demand for oil well cement to examine whether OBM cuttings can be used as a component of the raw meal in oil well cement manufacture.

2. Materials and Methods

2.1. Collection and preparation of raw materials

The primary raw materials required for cement manufacturing were collected at the Oman Cement Company (OCC). The conventional raw materials including limestone, quartz phyllite and iron ore mining come from within the company's immediate vicinity. For the current study, the required raw materials were collected from the stacked, homogenized piles from the OCC. The required amount of each material was then air-dried and crushed to a finer size using a lab-scale jaw crusher. These crushed materials, which were generally reduced to less than 5 mm in size, were used for the raw meal preparation. The raw meal was a mixture of all the raw materials mixed and further ground to a fine powder as per the raw mix design calculations. The OBM cuttings were collected from one of the OBM waste storage yards that are located at the *Fahud* oil production station (Petroleum Development Oman). Fig. 1 shows a typical drilling rig with OBM cutting waste generation process. The wet OBM cuttings from

drilling operations were transferred to designated landfills and were allowed to be dried by the direct sunlight. This air-drying process continues for a couple of years and the semi-dried OBM cuttings which possess moisture content up to 8% were collected and used for the current study.

2.2. Raw mix design

Depending on the type of cement, the ratios of raw materials vary. Table 1 shows a typical oil well cement composition. Raw material percentages were calculated using the allegation-alternate method of designing with multiple raw material component calculation system.

Based on this raw mix design calculation, the quantity of raw materials was calculated in percentages, and the mixture was mixed accordingly after weighing. The lime saturation factor (LSF), silica ratio (SR), and alumina ratio (AR) are the primary deciding calculation factors that determine the amount of raw materials to mix. The raw mixes were designed according to parameters that were based on the final cement product's chemical properties. Further, the design also considered fulfilling the mineralogical composition requirements after the sintering process like tri-calcium silicate (C_3S), dicalcium silicate (C_2S), tricalcium aluminate (C_3A), and tetra-calcium alumino ferrite (C_4AF). The calculation factor targets were as follows:

- Lime saturation factor (LSF): ≈ 92.0
- Silica ratio (SR): ≈ 2.6
- Alumina ratio (AR): ≈ 0.7

By designing the raw mix using five raw materials, including the research material OBM waste cutting according to the above parameters, the final oil well cement composition was determined. A total of six raw mixes, therefore, were designed and prepared with limestone

content ranging between 66.5–75.0%, OBM cutting content ranging between 5.0-20.0%, quartz phyllite in the range of 10.0–15.6%, and iron ore content between 3.3–3.5%.

2.3. Finer grinding process

The process of finer grinding is considered a vital part of the cement manufacturing process. Within the process, this size reduction stage occurs over several steps. For this study's purpose, finer grinding was performed at two levels:

- Raw materials grinding for raw meal preparation, and
- Cement grinding was carried out with produced oil well clinker and gypsum.

For this process of finer grinding stages, a TNS-50 drum mill (Siebtechnik Tema Inc., Cincinnati, Ohio, USA) was used. The material fed into the drum mill was pulverized by the freely moving grinding media through the action of pressure, impact, and shearing. Apart from size reduction, material homogenization was also carried out during the grinding process inside the cylindrical drum mill, which rotates around a fixed center point and is filled with different sized grinding media balls ranging in size from 5–50 mm. The machine has a volume of 55 dm^3, runs at 50 rpm, and has a grinding media weight capacity of 92 kg. Materials can be ground down to particles sized between ≈ 10 mm to less than ≈ 250 µm.

2.4. Characterization and testing

2.4.1. Chemical and mineralogical properties of raw materials and OBM cuttings

Raw materials and OBM cuttings are crushed in a lab jaw crusher and later pulverized to a fine powder for determining their chemical composition, which is generally carried out through wavelength dispersive X-ray spectrometry (WDXRF) or the wet method of analysis. WDXRF equipment is designed to carry out analyses using wavelength dispersion provided

196 with a set of fixed channels for each element. An X-ray tube under vacuum delivers fast and
197 reliable results.

198 Powdered samples mixed with a constant quantity of wax material can act as a binder;
199 in this study, the samples were further ground in an eccentric shaft grinding mill for a specified
200 duration. The powdered mix was then subjected to 15 kN of pressure using a hydraulic press
201 machine to make the material into a tablet form. This tablet then was fed into the WDXRF
202 machine for analysis, and the resulting kilo counts per second (kcps) were converted to a
203 concentration using a standard curve plotted using international standards.

204 The conventional wet-chemical method was used to determine the chemical
205 composition of the cement. Cement-related raw materials are generally tested through
206 gravimetry, and through titrimetric and complexometric methods to determine major
207 constituents. To determine minor elements, flame photometry for sodium and potassium, and
208 argentometry for chloride methods are used. Methods used to determine elements follow
209 ASTM and EN standard techniques using references for cement and cement related materials.
210 The OBM cuttings in this study were further tested through XRD, studied for their
211 mineralogical composition, and compared with limestone.

212

213 *2.4.2. Preparation of raw meal for sintering*

214 The raw meal powder samples were first mixed with water and shaped to 20–30 mm
215 size balls. These balls were then oven-dried for 24 hours to remove moisture. Hardened balls
216 were then subjected to heat treatment. All the samples were placed in a steel container and kept
217 inside the furnace. The temperature rose from room temperature to 1450 °C using a
218 programmable controller with an RTD sensor available with the equipment. After reaching the
219 set temperature, the samples were left alone for 30 minutes for chemical reactions and phase
220 formations to occur. After completing the heat treatment, clinker nodules were cooled rapidly

by an air blower and preserved in sealed bags for further processing. Produced clinker with different proportions of OBM cutting waste was then subjected to WDXRF, XRD (Fig. 2), and wet analysis to confirm and compare their compositions with conventional oil well clinker (RMX_{ref}).

2.4.3. Burnability and thermal analysis study

This study was based on determining uncombined CaO in the sintered raw mix (clinker) after a specific time and temperature. The raw mixes were subjected to thermal treatment at varying temperatures. The resulting clinker was then cooled rapidly and ground until it could pass through a 200 mesh to determine levels of uncombined/free CaO. The uncombined/free CaO was then extracted with hot moisture-free ethylene glycol and titrated with 0.1 N hydrochloric acid using bromocresol green as an indicator (IS: 4032, 1985). In this study, the analysis was carried out for clinker materials sintered at 1350, 1400 and 1450 °C. The results obtained for each raw mix were tabled and studied.

The measurement of heat flow and changes in weight associated with materials' transitions and reactions over the temperature in a controlled atmosphere is referred to as thermal analysis. The simultaneous testing of differential scanning calorimetry (DSC) and thermogravimetric analysis (TGA) offers higher productivity in the data analysis. The DSC technique determines variation in a sample's exothermic or endothermic heat flow during controlled thermal conditions while thermogravimetry measures a material's weight loss under the same thermal condition. The prepared raw and reference raw mixes were subjected to thermal treatment up to 1400 °C at a rate of 20 °C per minute, and the loss in weight and exo and endothermic behaviors was studied.

2.4.4. Physico-mechanical testing for OWC

2.4.4.1. Thickening time test

All the cements were transformed into a cement slurry for this testing by using distilled water in the ratio of 44% by mass to the cement. This slurry was tested under a specified temperature, and the pressure conditions and pumpability time were calculated by measuring the consistency according to the Bearden consistency (Bc) scale. The time after which the cement slurry consistency became high enough that the slurry became unpumpable was standardized as 100 Bc.

By using a blade-type mixing device, the researchers were able to mix cement and water at a 4,000 and 12,000 rpm rotational speed for 15 seconds and 30 seconds. The cement slurry was then prepared for further testing. A pressurized high-pressure, high-temperature consistometer (HPHT) capable of withstanding high temperatures and high pressure was used for the thickening time test. The HPHT was equipped with a heating system, and the pressure vessel was filled with synthetic oil for pressurizing. The slurry container, which held the cement slurry for testing, was equipped with a potentiometer which measured the consistency in Bc. The container was kept inside the HPHT pressure vessel and rotated at a speed of 150 rpm. When the Bc reached 100, the testing was completed, and the time taken to reach this value was noted and studied.

2.4.4.2. Free fluid (FF) test

This test determines the amount of colored or colorless water that separates from the cement slurry after keeping the cement slurry static for two hours in an Erlenmeyer flask. The cement slurry, which was prepared in a mixing device and transferred to an atmospheric consistometer, was stirred at 150 rpm and kept at a temperature of 27 °C in atmospheric pressure for 20 minutes. The conditioned slurry was then transferred to a 500 ml graduated

Erlenmeyer flask and kept on a vibration-free surface for two hours. After the required period, the supernatant water was pipetted out and measured. Using calculations, the quantity of FF was calculated by the percentage of the total derived and compared.

2.4.4.3. Slurry density test

Slurry density is the weight per unit volume of neat cement slurry and is generally given in units of lbm/gal or kg/m^3. It is one of the main parameters for well security and integrity. The slurry density varied based on the water-to-cement ratio per API classifications of the cement. The density ranged from 1380–2280 kg/m^3 or 11.5–19.0 lbm/gal (Schlumberger, 2019). It was measured using a fluid density balance to calculate the absolute density of the fluid sample. The cement slurry was placed in a fixed volume via a sample cup and pressurized to decrease the amount of entrained air. After preparation, the cement slurry was placed in a mixing device with 44% by mass of distilled water and then transferred to the sample cup of the fluid density balance. The Fann model 140 fluid density balance (Fann Instrument Company, Houston, Texas, USA) was used for testing and included a graduated balance beam with a cup, a sliding weight rider to achieve balance, a lid cap, a base with a fixed fulcrum, and a plunger. The plunger operated like a syringe and was used to pressurize the sample cup.

2.4.4.4. Rheology test

A study of rheological properties is a study of the flow of OWC slurry that determines the quality of the cement slurry and helps predict the end-use performance and physical parameters during handling and for the long term. The flow properties, in general, are affected by factors like water-to-cement (w/c) ratio, particle size, distribution of cement grains, and chemical composition of cement. This value is measured by inducing shear stress in a

commonly used coaxial cylinder geometry, which measures the rheological property of cement slurry as the material sheared by rotating one of the cylinders.

The cement water mix percentage of 44 as per API Spec 10A (2019) was based on the mass of dry cement measured with an accuracy of ± 0.5 grams taken. By using a Chandler constant speed mixer model 30–60, the cement slurry was prepared and then transferred to a temperature-controlled liquid bath in a container. The cement slurry was conditioned using a fixed blade assembly rotating at 150 rpm by the consistometer model-1200 (Chandler Engineering). The cement slurry was stirred for 20 minutes at a set temperature of 27 ± 2 °C at atmospheric pressure. This conditioned slurry was then transferred to a Fann viscometer (model 35SA) for studying the rheological behavior such as gel strength and viscosity. The viscosity caused by the viscous drag exerted by the slurry was transmitted to a precision spring and measured in centipoise or milli-Pascal seconds.

2.4.4.5. Compressive strength test

For the testing in the current study, an ELE-ADR model automatic compression machine connected with a 250 kN load frame was used. In this machine, the automated loading cycle system is controlled by a closed-loop microprocessor, and the hydraulic system operates based on a controlled loading rate. The device was fitted with a 50 mm square platen compression jig in accordance with ASTM C109 (2012) and API Spec 10A (2019) for testing the hydrated cement mortar. The cement slurry was prepared in a bottom-drive mixing device per standards and transferred and molded into a 50 × 50 mm cube. This cube mold was cured in a temperature-controlled water bath and crushed to determine compressive strength.

3. Results and discussion

3.1. Properties of raw materials

Chemical analysis of the primary raw materials is shown in Table 2. It can be seen that the limestone revealed a calcium content of 54.4%. The X-ray diffractometry (Fig. 3) identified the major calcium mineral formations as; calcite, calcitic dolomite, and dolomitic calcite, with calcite grain sizes ranging from 50–120 µm. Additionally, quartz (SiO_2) was identified as a predominant mineral, with ankerite and microcline present in minor proportions (Fig. 4). These calcite grains ranged from subhedral to euhedral and were distributed uniformly along with quartz, orthoclase-feldspar, and iron oxide.

The chemical composition of OBM cuttings contained 25.2% calcium (as CaO by XRF), while XRD revealed that this was primarily in the form of calcite, together with traces of dolomite. Other minerals present included quartz and muscovite, plus traces of talc, ankerite, and barite.

Iron was, unsurprisingly, the predominant element within the iron ore, at 58.3%. XRD revealed the presence of goethite, magnetite, and hematite. Quartz was observed as a minor mineral. XRF analysis of another fluxing additive, kaolin, indicated the presence of 32.7% as aluminum oxide and 39.7% as silicon dioxide. The mineral phases present were kaolinite, goethite, and quartz. The major silica source in the raw material was quartz phyllite, with 72.8% SiO_2 present in the form of quartz. Kaolinite, ankerite, muscovite, and hematite were also present as minor phases.

3.2. Raw mix analysis and thermal behavior

Table 3 shows different compositions of the designed raw mixes as limestone was replaced by OBM cuttings. Note that the proportions of the other raw materials also changed based on the required LSF, SR, and AR as detailed in Table 4. The resultant elemental

compositions of the six raw mixes are summarized in Table 5, which also shows the fluctuation in LSF for each mix, plus the slightly decreasing SR and increasing AR with increasing OBM cutting content. XRD study carried out to compare the prepared mixes (Fig. 5).

The decarbonation of calcite ($CaCO_3$) in all the mixes was compared via differential scanning calorimetry (Fig. 6). The derivative curves showed carbonate dissociation temperatures decreasing with increasing OBM cuttings content, which reduces fuel requirements. Further, the results showed that clinker phase formation started at lower temperatures, with a drop of 30 °C between the reference mix and RMX_6 (Fig. 7). This observation confirms the trends in free lime contents observed in the burnability test results.

Burnability, in general, is chiefly a measure of the ease of formation of the alite phase from belite with the free lime and other major phase formations like aluminate and ferrite. The importance of optimizing the burnability of clinker by tailoring the burning and sintering process stems from its potential for energy savings, production increases, and product enhancement (Hills et al., 2002). To determine the burnability of cement clinker, two different approaches were considered. These approaches would fundamentally satisfy the complexities of reactions and complex chemistry (Hewlett, 2003). According to this, the reaction kinetics carried out in the transformation from raw meal to clinker were classified as decomposition, diffusion, melting, liquid phase sintering, nucleation and crystal growth, polymorphic transformation, and condensation. Reaction kinetics are influenced considerably by their chemical, physical, and mineralogical characteristics and thus influence the quality of the final product.

With a thermal treatment of the raw mix samples at 1350, 1400 and 1450 °C, there was a decrease in free lime with increasing temperature for all raw mixes and references. Further, increased OBM levels led to a general (but not consistent) decrease in free lime. The effect of

364 OBM addition was greatest at lower temperatures. RMX_3 showed the lowest change of all the
365 samples because the LSF was lowest when compared to all other raw mixes.
366
367 *3.3. Particle size distribution and decarbonation*
368 Variations in decarbonation behavior were found to vary with particle size distribution
369 (PSD). This relates to the critical particle size, which is the maximum acceptable particle
370 diameter of the calcareous and siliceous compounds in raw meals to prevent any impairment
371 of burnability (Telschow, 2012). The smaller the particle size, the lower the energy requirement
372 for decarbonation. In general, the cement industry uses a ball and vertical roller mills for
373 particle size reduction. But costs and machinery efficiency prevent ideal particle sizes from
374 being attained. Despite this, 40% of the energy consumption in a typical cement plant is due to
375 grinding (Anon, 1993). The particle size distributions were modeled using the Rosin-Rammler
376 Distribution (RRD) function (Fig. 8). The data suggest that the slope of the cumulative
377 oversized distribution curves tended to increase in a range of 90–45 m as the percentage of
378 OBM cuttings increased. The finer particle size distribution (PSD) leads to a larger surface area
379 in the raw mix which favors a more rapid and high rate of heat transfer (Duda, 1975). For the
380 samples, the heat flow curve was obtained and transformed into second derivative curves,
381 which aided with easier data interpretation (Gabbott, 2008). The endothermic peak appears
382 inverted due to a second derivative function, which reflects a move towards a lower
383 temperature as the percentage of OBM cuttings increased in the raw mix.
384 The results in Table 6 showed significant variation in the burnability process according
385 to the percentage of OBM cutting in the raw mixes. Table 7 summarizes the calculated phases
386 with their compositions. On the other hand, the calcareous and siliceous materials in the OBM
387 cuttings differed in size, with finer particle sizes due to the rotary drilling technique. In general,
388 for oil well drilling, the cuttings along with drilling fluids that emerge allowed to settle in the

mud tank. They are then filtered using a sand separator, the contaminated mud is recirculated using a mud pump for drilling work. This process leads to finer silicate and calcite minerals in the rejected OBM cuttings (IOGP, 2016).

These OBM cuttings were used as a replacement for limestone with a reduction in particle size as the OBM cutting content increased. This correlated with the lowering of carbonate decomposition temperature. As per Taylor (1997), Fundal's equation (Eq. (1)) is used for defining burnability by using the percentage of free lime as,

$$CaO_{1400} = [0.343\,(LSF - 93) + 2.74(SR - 2.3)] + [0.83Q_{45} + 0.10C_{125} + 0.39R_{45}] \quad (1)$$

Where CaO_{1400} refers to free lime after burning at 1400 °C, LSF is the lime saturation factor, SR is the silica ratio, Q_{45} is the percentage of quartz over 45 microns, C_{125} is the percentage of calcite over 125 microns, and R_{45} is the percentage of other acid-insoluble residues over 45 microns. From Eq. (1), it is evident that the siliceous and calcareous materials' fineness played a critical role in controlling burnability, and these materials favor phase formation.

This endothermic decarbonation reaction rate also referred to as the Ginstling-Brounschtein relationship (Eq. (2)), is believed to give a better description of the overall decomposition process (Hewlett, 2003),

$$F(\alpha) = \left(1 - \frac{2}{3}\alpha\right) - (1 - \alpha)^{\frac{2}{3}} = \left(\frac{k}{r^2}\right)t \quad (2)$$

In Eq. (2), r is the particle radius, α is the fraction decomposed at some time t at a constant temperature, and k is a rate constant.

411 Even though there were variations in reactions based on thermochemical calculations,
412 the overall energy required for the clinkerization process remains unchanged. But on an
413 industrial scale, the changes in the rate of reactions increase clinker production to a reasonable
414 extent, including the rate of decarbonation as an important step.
415 The variation in the burnability of the raw mixes was also studied; the variability was
416 most evident in the raw mixture's 1350–1450 °C temperature range. The most abundant
417 minerals (i.e., CaO and SiO_2) reacted at this temperature range and resulted in the formation of
418 thermodynamically stable C_3S and C_2S phases. The rate of formation and disappearance of free
419 CaO related to the radius of the mineral particles; hence, the finer OBM cutting minerals
420 contributed to relatively higher phase formation. This finding was confirmed by the free CaO
421 determination of clinkers formed at different temperatures. The results were given in mixes,
422 and the tests were carried out as per the standard method (Lerch and Bogue, 1930).
423 The mineral barite ($BaSO_4$) is present in the OBM cuttings. The effects of barium (Ba)
424 on clinkerization have been studied by Xin et al. (2000) and Ludwig and Zhang (2015), who
425 revealed a decrease in phase formation temperature and an increase in compressive strength
426 when barium was present. As such, barium may be considered a mineralizer, which according
427 to Taylor (1997), is an agent that promotes the formation of a particular solid phase by affecting
428 the equilibria through incorporation in one or more of the solid phases. Katyal et al. (1999)
429 studied the effect of barium as a mineralizer on alite formation, finding that the presence of up
430 to 0.5% BaO in the raw mix acted as a mineralizer at 1450 °C and aided C_3S formation. XRD
431 analysis of OBM cuttings confirmed the presence of Ba in the form of $BaSO_4$, commercially
432 termed as barite. This is used as a weighing agent during drilling operations (Ibrahim et al.,
433 2017) due to its exceptionally high specific gravity (4.2–4.5). Zezulová et al. (2016) used 0.5-
434 5.0% barium sulfate and barium carbonate in the raw mix and studied phase formation. They
435 showed an increase in alite formation when up to 1% Ba was in the raw mix. This formulation

improved burnability due to the earlier melting of $BaSO_4$. But higher percentages of barium deteriorated the mineralogy.

In the solid-state reaction region (i.e., from 1200–1380 °C) before the formation of C_3S, the reaction between CaO with aluminates and the other silicates begins. The temperature of this process mainly depends on the liquid content and contributed to the SO_3, MgO, and minor elements apart from major oxides (Segata et al., 2019). These minor constituents support the earlier phase formation by acting as mineralizers and increasing the mobility of oxides in the liquid state. Al-Dhamri et al. (2019b) studied this effect of barium in clinker formation, while Katyal et al. (1999) studied the burnability of clinker with barium and showed that it acts as a mineralizer, accelerating the phase formation at earlier temperatures.

The mineralogical compositions of the clinkers were obtained after firing at 1450 °C for 30 minutes, from which theoretical C_3S and C_3A contents were determined (Table 8). The potential C_3S and C_3A contents were in the range of 52.95–57.01 and 0.65–2.50. Optical microscopy revealed that the alite and belite grains were distributed evenly, with an average alite grain size between 32–37 mm having a pseudohexagonal shape. Most belite grains ranged between 20–30 mm and were found as clusters and had a sub-rounded shape with corroded margins. The porosity of the clinker was high, and a considerable amount of interstitial matter was observed.

3.4. Physio-mechanical properties

Table 9 gives the elemental composition of each of the cements, together with the calculated phase composition. As a primary requirement for OWC, the physio-mechanical properties as per API specifications (Table 10) were conducted in all cements (API Spec 10A, 2019). The water/cement ratio was 0.44 % as recommended by the standard. To compare the

cements, the fineness was controlled for uniformity in testing and was in the range of 296–311 m^2/kg.

For the samples prepared with OBM cuttings, there was a steady decrease in slurry density (SD) with increasing OBM addition, falling from 16.4 for RMX_1 to 15.7 for RMX_5 and RMX_6. This was caused by the presence of non-hydrated cement in the cement slurry after mixing (Nelson and Guillot, 2006). However, the reference cement had a slurry density of 15.9, suggesting that it was the mixes with OBM cutting contents of up to 13% which deviated from expected behavior. Similarly, cements containing up to 13% showed free fluid values greater than that of the reference cement, while higher OBM cutting contents led to lower free fluid values, with a minimum at 15% OBM cutting (RMX_4). Thickening times based on Bearden's consistency varied from 93 to 117 Bc and were within the limits of a Class G well cement condition of 90 to 120 Bc. Compressive strengths decreased consistently at 38 °C with increasing OBM cutting content and showed a general downwards trend at 60 °C. However, only the RMX_6 failed the standard requirement. All of the cements exhibited similar rheological behavior (Table 11). The viscosity and gel strengths confirmed less gelation of cement slurries, a prime requirement for pumping cement slurries during operation.

3.5. Cement hydration

The cement hydration carried out showed good similarities in all raw mixes with $RMX_{ref,}$ and the obtained results are plotted in Fig. 9. The hydrated cement samples were kept in tightly closed vials in required environmental conditions. When tested using thermal studies, the TGA–DSC calorimetry showed the RMX_{ref} was highest for CH and CH_{eq} formation on days two, seven, and twenty-eight. After seven days, the RMX_{ref} showed the highest value and RMX_5 showed the lowest. This finding may be due to the lower LSF and C_3S contents; the higher proportion of C_2S that formed in the cement, and the slower rate at which the cement

485 hydrated (Puertas et al., 2010). The thermal curve showed three different curves for the
486 hydrated cement test with weight losses in ettringite, portlandite, and calcite in the ranges of
487 110-120, 200-400 and 580-900 °C, respectively (Bullard et al., 2011). The remaining RMXs
488 were almost on the same levels of formations and displayed slight variations according to their
489 mineralogical composition. In the study group, RMX_3, when compared to other raw mixes,
490 displayed a lower C_3S content when compared to all other cements.

491 At twenty-eight days, the hydration behavior of CH, and CH_{eq} formation showed an
492 increasing trend as the OBM cuttings percentage increased and then at 20%, it showed a
493 reduction. The reduction of CH and CH_{eq} formation may be due to a reduction in C_3S and C_2S
494 minerals as most of the calcium converted to C_3A and C_4AF, which generally does not
495 contribute to strength (Chen and Juenger, 2009). The hydration of all cements manufactured
496 with different percentages of OBM indicates that the behavior was similar to commercial
497 references. The portlandite formation for all the cements was higher at the early stages of
498 hydration, and at later stages, ettringite formation increased (Gabrovšek et al., 2006). An
499 increase in C-S-H portlandite formation was observed at twenty-eight days with hydrated
500 cement using XRD (Fig. 10), which confirms that OBM cutting replacement in the cement
501 favors the hydration process.

502 The hydration of OWCs at different stages was calculated (Table 12). This study's
503 findings also confirm that there is not much of a difference in earlier hydration of all cements
504 used for reference. Among all samples, the reference showed high hydration levels at two,
505 seven and twenty-eight days, followed by RMX_4 and RMX_5. Later hydration at seven and
506 twenty-eight days in RMX_4 and RMX_5 almost matched the hydration of RMX_{ref}.
507

4. Conclusions and future prospects

The cement prepared using OBM cuttings had very similar rheological properties as the manufactured industrial well cement. This finding suggests that OBM cuttings could be used to produce OWC. The most important results of this study are listed below:

- All clinker phases were well-formed and had concentrations that met clinker requirements for producing OWC.
- The addition of OBM cuttings reduced the calcination temperature, granting two advantages. First, reducing calcination temperature also lowers fuel consumption during manufacturing. Second, lower CO_2 emissions result from such a process due to a reduction in the amount of fuel required.
- The burnability of the raw meal with a higher percentage of OBM cuttings resulted in lower free lime content, indicating the improved burnability behavior of raw meal when OBM cuttings were added.
- As the OBM cuttings increased, the resultant OWC had lower compressive strength. Substituting up to 15% of OBM cuttings in cement meets compressive strength requirements.
- Above 15% OBM cuttings substitution, the alite content was reduced as a result of a lower LSF, leading to a compressive strength which was below the standard requirement.
- Proper study on the calcium content of the available OBM cuttings is suggested to be prepared. Based on this, the raw mix design will be prepared for manufacturing on an industrial scale.
- Plant level studies are suggested to be accomplished for the practical implementation of the study, and this, in turn, will benefit industries to a greater extent.

Acknowledgments

The research leading to these outcomes has received Research Project Funding from The Research Council of the Sultanate of Oman (TRC), Research Agreement No. ORG/SQU/ei/15/009.

Conflict of Interest

The authors declare no conflict of interest regarding this article's publication.

References

Abdul-Wahab, S.A., Al-Rawas, G.A., Ali, S., Al-Dhamri, H., 2016. Impact of the addition of oil-based mud on carbon dioxide emissions in a cement plant. J. Clean. Prod. 112, 4214–4225. https://doi.org/10.1016/j.jclepro.2015.06.062.

Al-Dhamri, H.S., Abdul-Wahab, S.A., Velis, C., Black, L., 2019a. Oil-based mud cutting as an additional raw material in clinker production. J. Hazard. Mater. 121022. https://doi.org/10.1016/j.jhazmat.2019.121022.

Al-Dhamri, H., Abdul-Wahab, S., Ram, G., Al-Moqbali, A., Black, L., 2019b. Microstructure of clinker prepared using different ratio of OBM cutting as raw material, 15th International Congress on the Chemistry of Cement.

Al-Futaisi, A., Jamrah, A., Yaghi, B., Taha, R., 2007. Assessment of alternative management techniques of tank bottom petroleum sludge in Oman. J. Hazard. Mater. 141, 557–564. https://doi.org/10.1016/j.jhazmat.2006.07.023.

Allers, E., Abed, R.M.M., Wehrmann, L.M., Wang, T., Larsson, A.I., Purser, A., de Beer, D., 2013. Resistance of Lophelia pertusa to coverage by sediment and petroleum drill cuttings. Mar. Pollut. Bull. 74, 132–140. https://doi.org/10.1016/j.marpolbul.2013.07.016.

Anon, 1993. Reducing specific power usage in cement plants, in: World Cement. pp. 25, 27–28, 30, 32–35.

API Spec 10A, 2019. Specification for Cements and Materials for Well Cementing, Twenty-Fifth Edition.

ASTM, 2012. Standard test method for compressive strength of hydraulic cement mortars (Using 2-in . or 50-mm cube specimens). ASTM International.

Ayati, B., Molineux, C., Newport, D., Cheeseman, C., 2019. Manufacture and performance of lightweight aggregate from waste drill cuttings. J. Clean. Prod. 208, 252–260. https://doi.org/10.1016/j.jclepro.2018.10.134.

Barthel, M., Rübner, K., Kühne, H.-C., Rogge, A., Dehn, F., 2016. From waste materials to products for use in the cement industry. Adv. Cem. Res. 28, 458–468. https://doi.org/10.1680/jadcr.15.00149.

BP Statistical Review of World Energy, 2019. https://www.bp.com/content/dam/bp/business-sites/en/global/corporate/pdfs/energy-economics/statistical-review/bp-stats-review-2019-full-report.pdf.

Bullard, J.W., Jennings, H.M., Livingston, R.A., Nonat, A., Scherer, G.W., Schweitzer, J.S., Scrivener, K.L., Thomas, J.J., 2011. Mechanisms of cement hydration. Conf. Spec. Cem. Hydration Kinet. Model. Quebec City, 2009 CONMOD10, Lausanne, 2010. https://doi.org/10.1016/j.cemconres.2010.09.011.

Chatterjee, A.K., 2018. Cement Production Technology: Principles and Practice. CRC Press.

Chen, I.A., Juenger, M.C.G., 2009. Incorporation of waste materials into portland cement clinker synthesized from natural raw materials. J. Mater. Sci. 44, 2617–2627. https://doi.org/10.1007/s10853-009-3342-x.

Davies, J.M., Addy, J.M., Blackman, R.A., Blanchard, J.R., Ferbrache, J.E., Moore, D.C., Somerville, H.J., Whitehead, A., Wilkinson, T., 1984. Environmental effects of the use of oil-based drilling muds in the North Sea. Mar. Pollut. Bull. 15, 363–370. https://doi.org/10.1016/0025-326X(84)90169-3.

Dow, F.K., Davies, J.M., Raffaelli, D., 1990. The effects of drill cuttings on a model marine sediment system. Mar. Environ. Res. 29, 103–134. https://doi.org/10.1016/0141-1136(90)90031-I.

Duda, W.H., 1975. Dudaa. Cement-Data-Book, Vol-1.

591 Gabbott, P., 2008. A Practical Introduction to Differential Scanning Calorimetry. Princ. Appl.
592 Therm. Anal. 1–50. https://doi.org/10.1002/9780470697702.ch1.
593 Gabrovšek, R., Vuk, T., Kaučič, V., 2006. Evaluation of the hydration of Portland cement
594 containing various carbonates by means of thermal analysis. Acta Chim. Slov. 53, 159–
595 165.
596 Hewlett, P.C., 2003. Lea's Chemistry of Cement and Concrete, Lea's Chemistry of Cement
597 and Concrete. Elsevier. https://doi.org/10.1016/B978-0-7506-6256-7.X5007-3.
598 Hills, L. M., Johansen, V., MacGregor, F.M., 2002. Burning the mix. International Cement
599 Review.https://www.cemnet.com/public/courses/srm01L1/story_content/external_file
600 s/burning-the-mix.pdf (accessed 20 November 2019).
601 Ibrahim, D.S., Sami, N.A., Balasubramanian, N., 2017. Effect of barite and gas oil drilling fluid
602 additives on the reservoir rock characteristics. J. Pet. Explor. Prod. Technol. 7, 281–292.
603 https://doi.org/10.1007/s13202-016-0258-2.
604 IOGP, 2016. Drilling waste management technology review.
605 https://www.iogp.org/bookstore/product/drilling-waste-management-technology-
606 review/.
607 IS: 4032, B. of I.S., 1985. IS: 4032-1985, Method of Chemical analysis of Hydraulic Cement,
608 Indian Standard.
609 Katyal, N.K., Ahluwalia, S.C., Parkash, R., 1999. Effect of barium on the formation of
610 tricalcium silicate. Cem. Concr. Res. 29, 1857–1862. https://doi.org/10.1016/S0008-
611 8846(99)00172-6.
612 Lerch, W., Bogue, R.H., 1930. Revised Procedure for the Determination of Uncombined Lime
613 in Portland Cement. Ind. Eng. Chem. Anal. Ed. 2, 296–298.
614 https://doi.org/10.1021/ac50071a036.
615 Li, X. G., Lv, Y., Ma, B. G., Jian, S. W., Tan, H. B., 2011. Influence of sintering temperature
616 on the characteristics of shale brick containing oil well-derived drilling waste. Environ.
617 Sci. Pollut. Res. 18(9), 1617-1622. https://doi.org/10.1007/s11356-011-0526-0.
618 Ludwig, H.M., Zhang, W., 2015. Research review of cement clinker chemistry. Cem. Concr.
619 Res. 78, 24–37. https://doi.org/10.1016/j.cemconres.2015.05.018.
620 Mostavi, E., Asadi, S., Ugochukwu, E., 2015. Feasibility Study of the Potential Use of Drill
621 Cuttings in Concrete. Procedia Eng. 118, 1015–1023.
622 https://doi.org/10.1016/j.proeng.2015.08.543.
623 Nelson, E., Guillot, D., 2006. Well Cementing: Second Edition, Second. ed, Schlumberger.
624 Puertas, F., García-Díaz, I., Palacios, M., Gazulla, M.F., Gómez, M.P., Orduña, M., 2010.
625 Clinkers and cements obtained from raw mix containing ceramic waste as a raw material.
626 Characterization, hydration and leaching studies. Cem. Concr. Compos. 32, 175–186.
627 https://doi.org/10.1016/j.cemconcomp.2009.11.011.
628 Schlumberger, 2019. Oil Field Glossary - Slurry Density
629 https://www.glossary.oilfield.slb.com/en/Terms/s/slurry_density.aspx.
630 Segata, M., Marinoni, N., Galimberti, M., Marchi, M., Cantaluppi, M., Pavese, A., De, Á.G.,
631 2019. Materials Characterization The effects of MgO, Na_2O, and SO_3 on industrial
632 clinkering process : phase composition, polymorphism, microstructure, and hydration,
633 using a multidisciplinary approach 155. https://doi.org/10.1016/j.matchar.2019.109809.
634 Shon, C.S., Estakhri, C.K., Lee, D., Zhang, D., 2016. Evaluating feasibility of modified drilling
635 waste materials in flexible base course construction. Constr. Build. Mater. 116, 79–86.
636 https://doi.org/10.1016/j.conbuildmat.2016.04.100.
637 Siddique, S., Kwoffie, L., Addae-Afoakwa, K., Yates, K., Njuguna, J., 2017. Oil Based Drilling
638 Fluid Waste: An Overview on Environmentally Persistent Pollutants. IOP Conf. Ser.
639 Mater. Sci. Eng. 195. https://doi.org/10.1088/1757-899X/195/1/012008.
640

Taylor, H.F.W. 1997. Cement Chemistry, 2nd edition. ed, Thomas Telford. Thomas Telford Publishing, London.
Telschow, S., 2012. Clinker Burning Kinetics and Mechanism.
The International Energy Agency, 2019. Global Energy & CO_2 Status Report 2018 https://www.iea.org/geco/data/.
Van Oss, H.G., Padovani, A.C., 2002. Cement manufacture and the environment - Part I: Chemistry and technology. J. Ind. Ecol. https://doi.org/10.1162/108819802320971650.
Xin, C., Jun, C., Lingchao, L., Futian, L., Bing, T., 2000. Study of Ba-bearing calcium sulphoaluminate minerals and cement. Cem. Concr. Res. 30, 77–81. https://doi.org/10.1016/S0008-8846(99)00204-5.
Zezulová, A., Staněk, T., Opravil, T., 2016. The Influence of Barium Sulphate and Barium Carbonate on the Portland Cement. Procedia Eng. 151, 42–49. https://doi.org/10.1016/j.proeng.2016.07.358.
Zhang, J., Weissinger, E.A., Peethamparan, S., Scherer, G.W., 2010. Early hydration and setting of oil well cement. Cem. Concr. Res. 40, 1023–1033. https://doi.org/10.1016/j.cemconres.2010.03.014.

LIST OF TABLE TITLES

LIST OF FIGURE CAPTIONS

686 **Table 1**
687 Typical mineralogical composition of oil well cement Class 'G'.

Oxide composition	Cement notation	Common name	Concentration (wt.%)
$3CaO \bullet SiO_2$	C_3S	Alite	48.0 – 58.0
$2CaO \bullet SiO_2$	C_2S	Belite	18.0 – 28.0
$3CaO \bullet Al_2O_3$	C_3A	Aluminate	<3.0
$4CaO \bullet Al_2O_3 \bullet Fe_2O_3$	C_4AF	Ferrite	12.0 – 18.0

688

689

690 **Table 2**
691 Chemical composition of raw materials (wt.%).

Material	LOI_{950}	SiO_2	Al_2O_3	Fe_2O_3	CaO	MgO	SO_3	Na_2O	K_2O	TiO_2	P_2O_5	Mn_2O_3
Limestone	42.55	1.82	0.20	0.45	54.42	0.15	0.15	0.18	0.04	0.03	0.00	0.00
OBM cuttings	30.91	22.65	8.53	3.89	25.16	1.31	2.10	0.90	0.88	0.98	0.32	0.05
Iron ore	10.25	16.15	10.75	58.32	1.21	0.79	0.08	0.18	0.10	0.66	0.21	0.57
Kaolin	13.23	39.67	32.76	8.81	1.53	0.36	0.12	1.02	0.13	2.03	0.03	0.03
QPh	3.20	72.87	7.11	6.03	5.27	2.85	0.09	1.02	0.74	0.57	0.08	0.11

692

693

694

695 **Table 3**
696 The proportion of raw materials in the designed raw mixes.

Raw material	Raw Material Proportion, %					
	RMX1	RMX2	RMX3	RMX4	RMX5	RMX6
Limestone	75.0	71.5	70.0	69.3	67.2	66.5
OBM cuttings	5.0	11.0	13.0	15.0	18.0	20.0
QPh	15.6	14.3	13.5	12.1	10.8	10.0
Iron ore	3.3	3.2	3.5	3.6	3.5	3.5
Kaolin	1.1	0.0	0.0	0.0	0.0	0.0

697

698

699 **Table 4**
700 Target parameters for raw mix design.

Parameter	Value
Raw mix residue on 90μ (R_{90})	10.0-13.0 %
LSF (lime saturation factor)	~92.0%
AR (alumina ratio)	~0.7%
SR (silica ratio)	~2.6%
C_3A content of clinker	< 1.0%
Free lime content of clinker	<1.5%

701

702

703

Table 5

Chemical composition of the designed raw mixes (wt.%).

Oxides	Blank (Bk)	RMX1	RMX2	RMX3	RMX4	RMX5	RMX6
LOI_{950}	34.73	34.44	34.61	34.59	34.88	35.07	35.16
SiO_2	15.21	14.83	14.73	14.62	14.06	13.74	13.59
Al_2O_3	2.05	2.40	2.44	2.59	2.67	2.81	2.93
Fe_2O_3	3.50	3.49	3.48	3.68	3.72	3.70	3.72
CaO	42.84	42.95	42.47	42.12	42.17	41.98	41.79
MgO	0.78	0.69	0.68	0.69	0.67	0.67	0.67
SO_3	0.02	0.24	0.35	0.39	0.43	0.49	0.53
Na_2O	0.07	0.36	0.38	0.39	0.39	0.40	0.41
K_2O	0.30	0.19	0.23	0.25	0.25	0.27	0.28
LSF	91.00	91.74	91.02	90.22	93.19	92.98	94.28
SR	2.70	2.52	2.49	2.34	2.20	2.21	2.01
AR	0.60	0.69	0.70	0.70	0.72	0.72	0.79

729 **Table 6**
730 Burnability evaluation of designed raw mixes with free CaO.

Mix No.	Burnability (% free CaO)		
	1350 °C	1400 °C	1450 °C
RMX1	1.92	1.26	0.90
RMX2	1.99	1.20	0.95
RMX3	1.81	1.00	0.94
RMX4	1.33	1.15	0.67
RMX5	1.40	0.93	0.75
RMX6	1.26	0.95	0.84

731

732 **Table 7**

733 Chemical composition of laboratory fired clinkers (wt.%).

Oxides	Blank-Bk	RMX1-CL	RMX2-CL	RMX3-CL	RMX4-CL	RMX5-CL	RMX6-CL
LOI_{950}	0.25	0.11	0.07	0.09	0.21	0.20	0.20
SiO_2	21.97	22.85	22.72	22.60	21.88	21.51	21.20
Al_2O_3	3.53	3.60	3.60	3.77	4.17	4.38	4.58
Fe_2O_3	5.46	5.26	5.16	5.51	5.58	5.58	5.70
CaO	64.90	65.50	65.06	64.69	64.64	64.38	64.35
MgO	1.24	1.10	1.02	1.06	1.06	1.04	1.08
SO_3	0.10	0.32	0.50	0.55	0.46	0.51	0.51
Na_2O	0.16	0.53	0.57	0.59	0.54	0.48	0.45
K_2O	0.23	0.29	0.37	0.37	0.25	0.21	0.21
Free lime	0.48	0.90	0.95	0.94	0.67	0.75	0.84
LSF	93.75	91.11	90.86	90.18	92.13	92.76	93.46
SR	2.44	2.58	2.59	2.44	2.24	2.16	2.06
AR	0.65	0.68	0.70	0.68	0.75	0.78	0.80
C_3S	63.76	56.66	55.29	52.95	56.79	56.66	57.01
C_2S	14.89	22.79	23.45	24.87	19.91	18.95	17.79
C_3A	0.11	0.65	0.82	0.68	1.62	2.18	2.50
C_4AF	16.62	16.01	15.70	16.77	16.98	16.98	17.35
Liquid	24.51	25.06	24.94	26.24	27.46	28.00	28.83

734

735

736 **Table 8**
737 Mineralogy composition of laboratory fired clinkers.

Sample No.	Phases Present	Quantity (%)	Granulometry (μ)		
			Min.	Max.	Avg.
CL/RMX1	Alite	52	2	78	36
	Belite	30	2	57	27
	Interstitial matter	18	-	-	-
CL/RMX2	Alite	50	2	82	37
	Belite	33	2	52	25
	Interstitial matter	17	-	-	-
CL/RMX3	Alite	48	2	74	32
	Belite	33	2	63	26
	Interstitial matter	19	-	-	-
	Alite	55	1	73	32
CL/RMX4	Belite	25	1	44	21
	Interstitial matter	20	-	-	-
	Alite	51	1	82	34
CL/RMX5	Belite	28	1	52	24
	Interstitial matter	21	-	-	-
	Alite	53	1	91	36
CL/RMX6	Belite	26	1	56	25
	Interstitial matter	21	-	-	-

738

739

740 **Table 9**
741 Chemical composition of oil well cement (wt.%).

Constituent/ Parameter	Blank-Bk	RMX1-CM	RMX2-CM	RMX3-CM	RMX4-CM	RMX5-CM	RMX6-CM
LOI_{950}	1.13	0.82	0.79	0.75	0.93	0.81	0.86
SiO_2	21.85	21.73	21.91	21.82	21.60	21.17	21.11
Al_2O_3	3.38	3.65	3.78	3.96	3.99	4.20	4.35
Fe_2O_3	5.37	4.92	5.00	5.32	5.48	5.39	5.43
CaO	62.95	62.65	62.65	62.87	63.02	62.58	62.39
MgO	1.19	1.12	1.05	1.08	1.01	0.96	0.99
SO_3	1.39	1.66	1.53	1.56	1.76	1.83	1.84
Na_2O	0.12	0.24	0.25	0.25	0.33	0.34	0.33
K_2O	0.25	0.18	0.16	0.17	0.15	0.18	0.16
LSF	90.18	90.06	89.07	89.14	89.77	90.39	90.04
SR	2.50	2.54	2.50	2.35	2.28	2.21	2.16
AR	0.63	0.74	0.76	0.74	0.73	0.78	0.80
C_3S	59.75	58.80	55.92	55.83	57.68	57.88	56.49
C_2S	17.59	17.96	20.65	20.46	18.43	17.06	17.93
C_3A	0.00	1.36	1.57	1.50	1.31	2.02	2.35
C_4AF	16.32	14.96	15.20	16.17	16.66	16.39	16.51
$2C_3A+C_4AF$	16.32	17.67	18.33	19.18	19.28	20.43	21.21

742

743

744 **Table 10**
745 Physical properties of oil well cement.

	Blank	RMX1	RMX2	RMX3	RMX4	RMX5	RMX6
Fineness (m^2/kg)	298	296	301	311	298	308	302
% passing on							
250 μ	100	100	100	100	100	100	100
212 μ	100	99.9	99.8	99.4	99.6	9.6	99.7
150 μ	99.3	99.3	99.1	98.3	98.7	98.6	98.9
90 μ	96.6	94.3	93.7	92.2	93.6	93.3	93.9
75 μ	81.4	84.8	83.9	81.8	84.4	83.8	84.7
63 μ	72.7	70.7	69.7	66.5	70.7	69.3	70.7
45 μ	45.6	48.6	47.5	42.9	48.1	46.3	48.0
38 μ	21.3	22.4	20.7	14.5	20.1	17.7	19.9
Slurry density @ 0.44% water	15.9	16.4	16.5	16.1	15.8	15.7	15.7
Free fluid (%)	5.0	5.8	5.6	5.3	3.8	4.3	4.4
Thickening time (Bc)	98	93	112	117	102	101	98
Compressive strength (psi)							
38 °C	581	558	477	412	404	389	292
60 °C	1930	1706	1645	1600	1660	1626	1466

746
747
748
749
750
751
752

Table 11
Rheology report of oil well cements.

Rheology parameters	Blank	RMX1	RMX2	RMX3	RMX4	RMX5	RMX6
Fann Viscometer							
600 rpm	116	89	102	104	104	126	113
300 rpm	92	64	78	70	87	101	86
200 rpm	82	56	65	61	79	83	79
100 rpm	69	45	45	51	68	69	68
6 rpm	31	28	25	25	28	30	29
3 rpm	18	19	16	16	17	19	18
Gel strength							
10 sec	19	16	18	16	18	20	19
10 min	22	19	19	23	22	23	22

770

771 **Table 12**

772 TG - hydration calculation for cements.

Sample		Weigh loss (Ettringite) %	Weigh loss (Portlandite) %	Weigh loss (Dolomite) %	W_f	[CH]	$[CH]_{eq}$	[CH] + $[CH]_{eq}$
		$a = (T_{f1} - Ti_1)$	$x = (T_{f2} - Ti_2)$	$y = (T_{f3} - Ti_3)$		$((74/18)*x)/W_f$	$((100/44)\ y\ (74/100))/W_f$	
2 Days	C_{Bk}	4.173	3.107	0.4815	74.41	0.1717	0.0109	0.1825
	C_{RM1}	6.2	2.73	0.4808	77.33	0.1451	0.0105	0.1556
	C_{RM2}	3.78	2.73	0.6752	78.5	0.1430	0.0145	0.1574
	C_{RM3}	5.408	2.404	0.3661	72.23	0.1368	0.0085	0.1454
	C_{RM4}	4.321	2.718	0.4752	72.17	0.1548	0.0111	0.1659
	C_{RM5}	4.372	2.735	0.5679	72.73	0.1546	0.0131	0.1677
	C_{RM6}	4.443	2.682	0.3769	73.86	0.1493	0.0086	0.1579
7 Days	C_{Bk}	6.278	4.513	1.672	76.75	0.2417	0.0366	0.2784
	C_{RM1}	4.483	2.856	0.5054	82.07	0.1431	0.0104	0.1534
	C_{RM2}	5.707	3.795	1.539	80.63	0.1935	0.0321	0.2256
	C_{RM3}	5.799	3.532	0.6074	74.64	0.1945	0.0137	0.2082
	C_{RM4}	5.561	3.811	0.6882	74.6	0.2100	0.0155	0.2255
	C_{RM5}	5.443	3.716	0.5476	72.94	0.2094	0.0126	0.2221
	C_{RM6}	4.946	3.534	1.933	78.1	0.1860	0.0416	0.2277
28 Days	C_{Bk}	7.305	4.907	1.692	75.24	0.2681	0.0378	0.3059
	C_{RM1}	6.142	4.361	1.139	75.18	0.2385	0.0255	0.2640
	C_{RM2}	5.489	4.517	0.9847	74.53	0.2492	0.0222	0.2714
	C_{RM3}	6.001	4.56	0.9668	75.04	0.2498	0.0217	0.2715
	C_{RM4}	5.696	4.478	2.047	75.11	0.2451	0.0458	0.2909
	C_{RM5}	6.744	4.867	0.7835	73.04	0.2739	0.0180	0.2920
	C_{RM6}	6.174	4.519	0.8056	72.25	0.2571	0.0188	0.2759

773
774
775
776
777
778
779
780
781
782

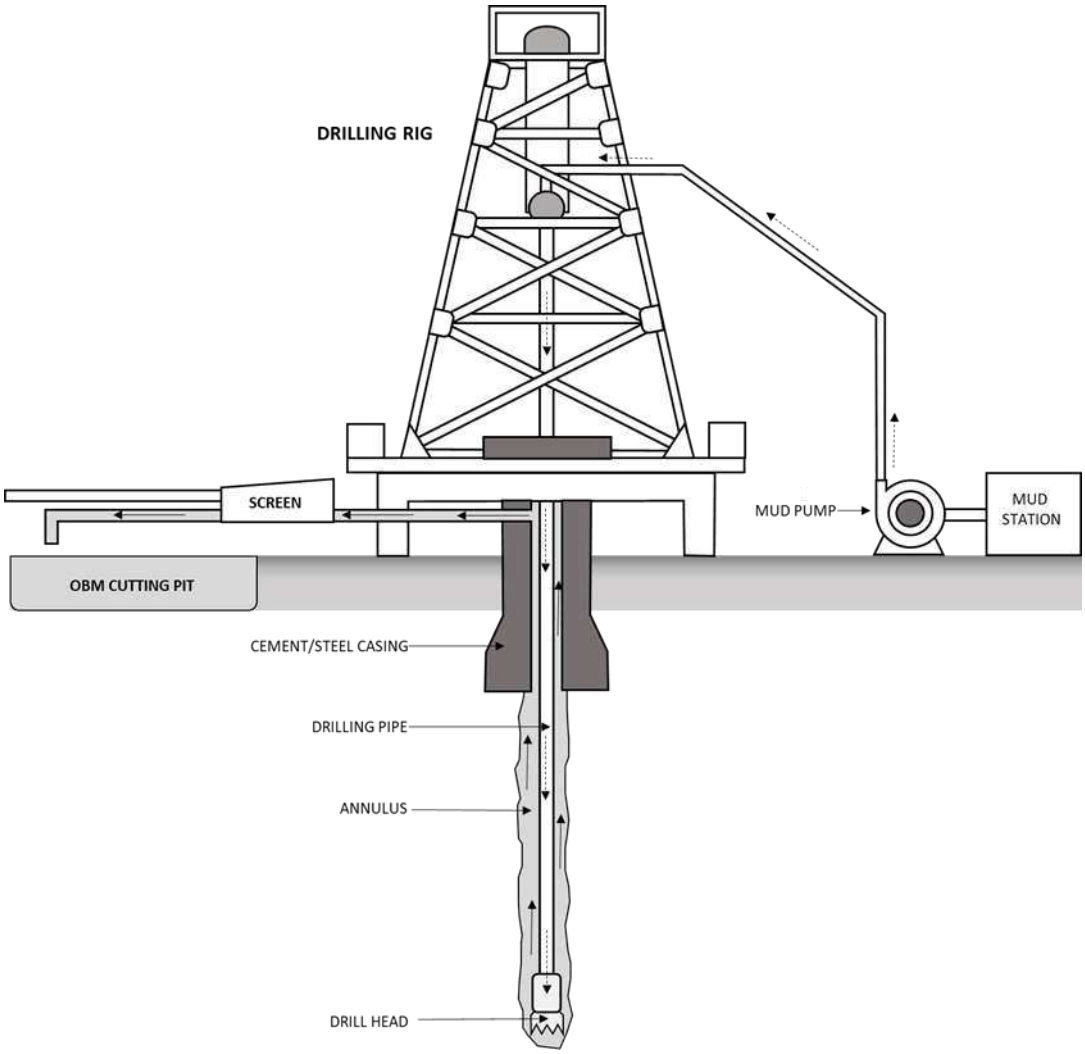

Fig. 1. Oil rig with OBM cutting collection pit.

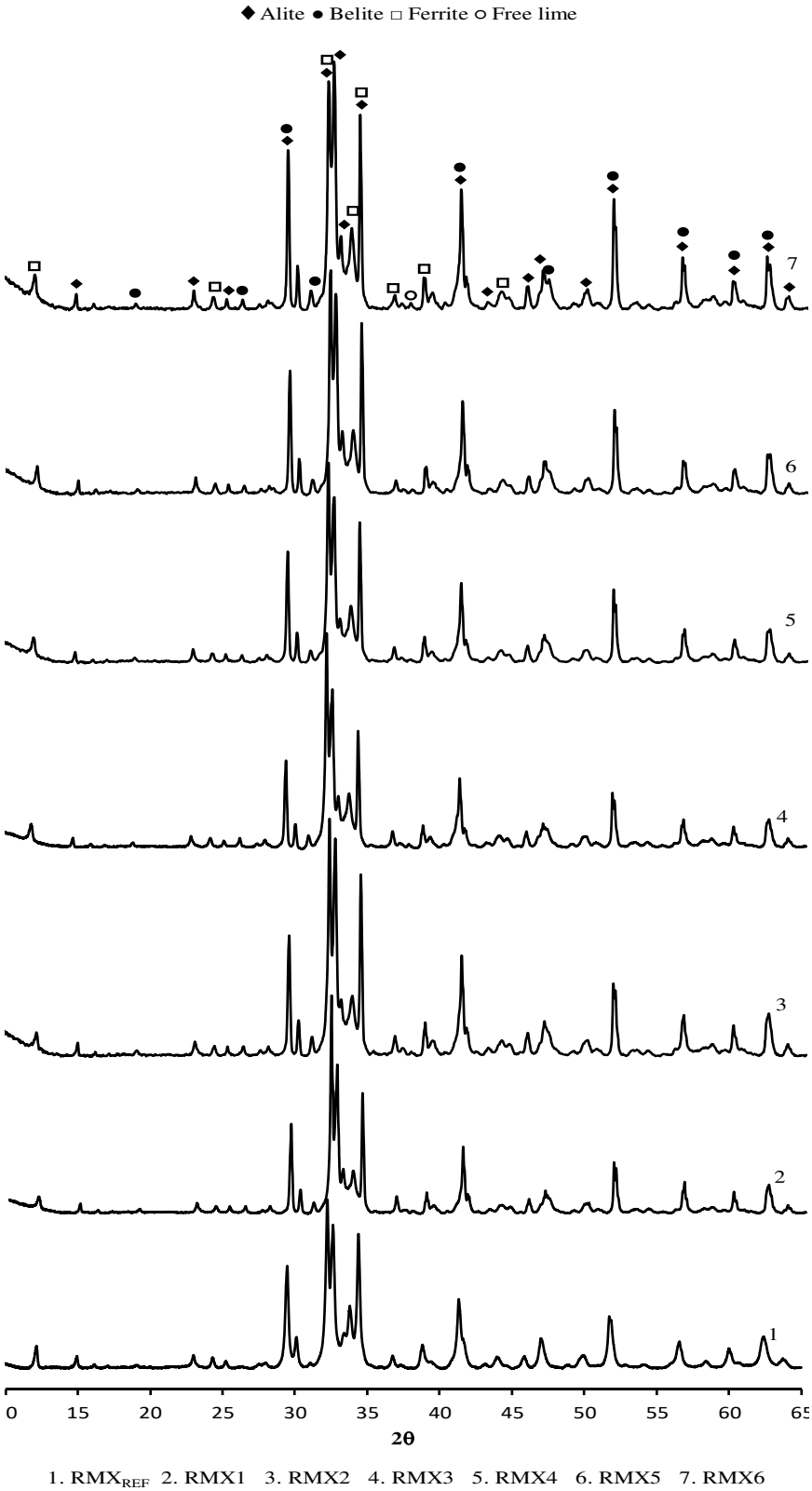

Fig. 2. Clinker X-ray diffractometry.

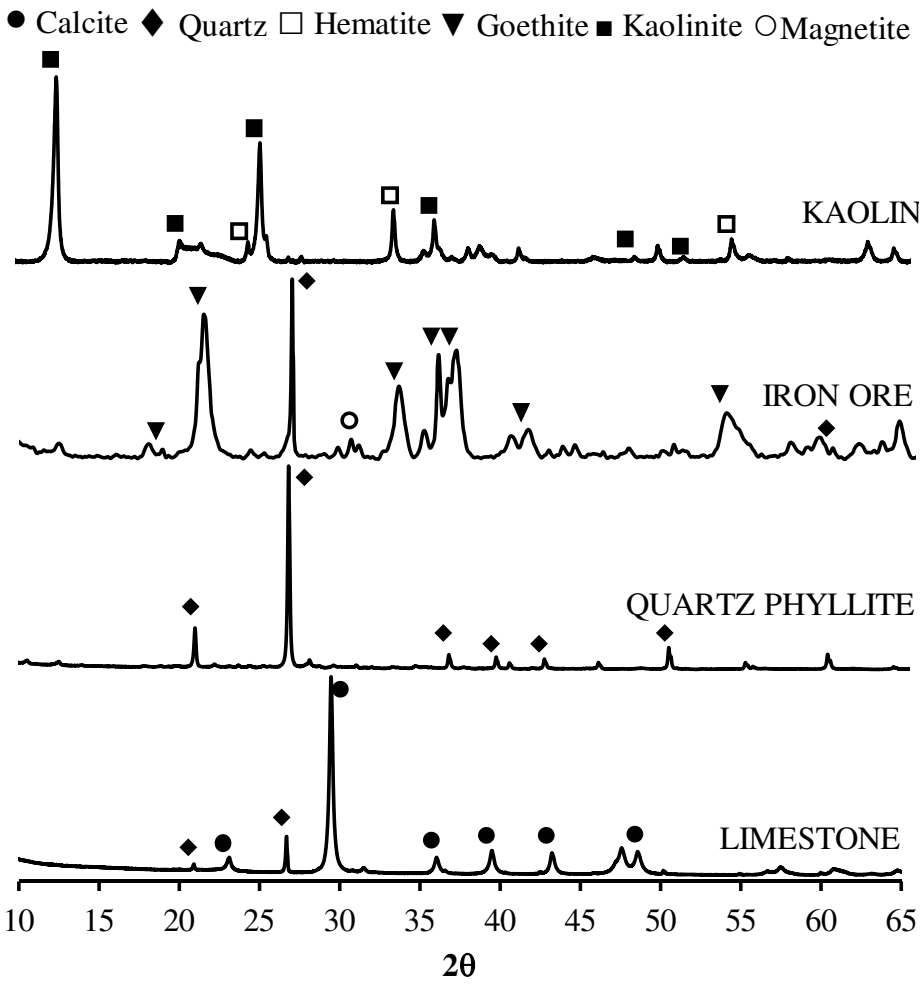

Fig. 3. Raw materials X-ray diffractometry.

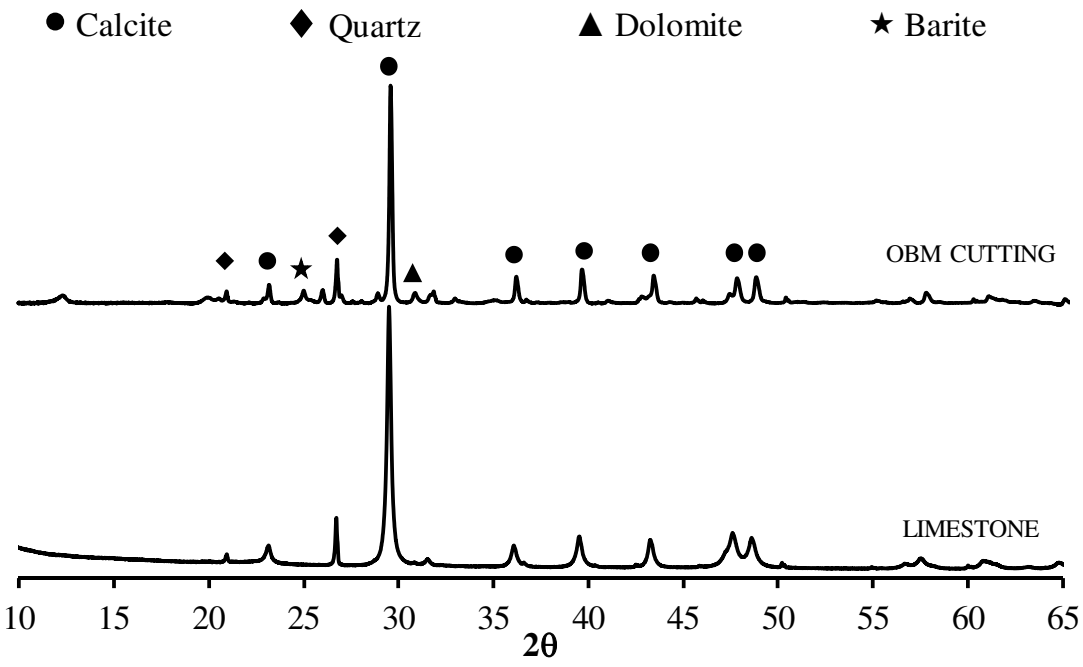

Fig. 4. Correlation in the mineralogy of limestone and OBM cuttings.

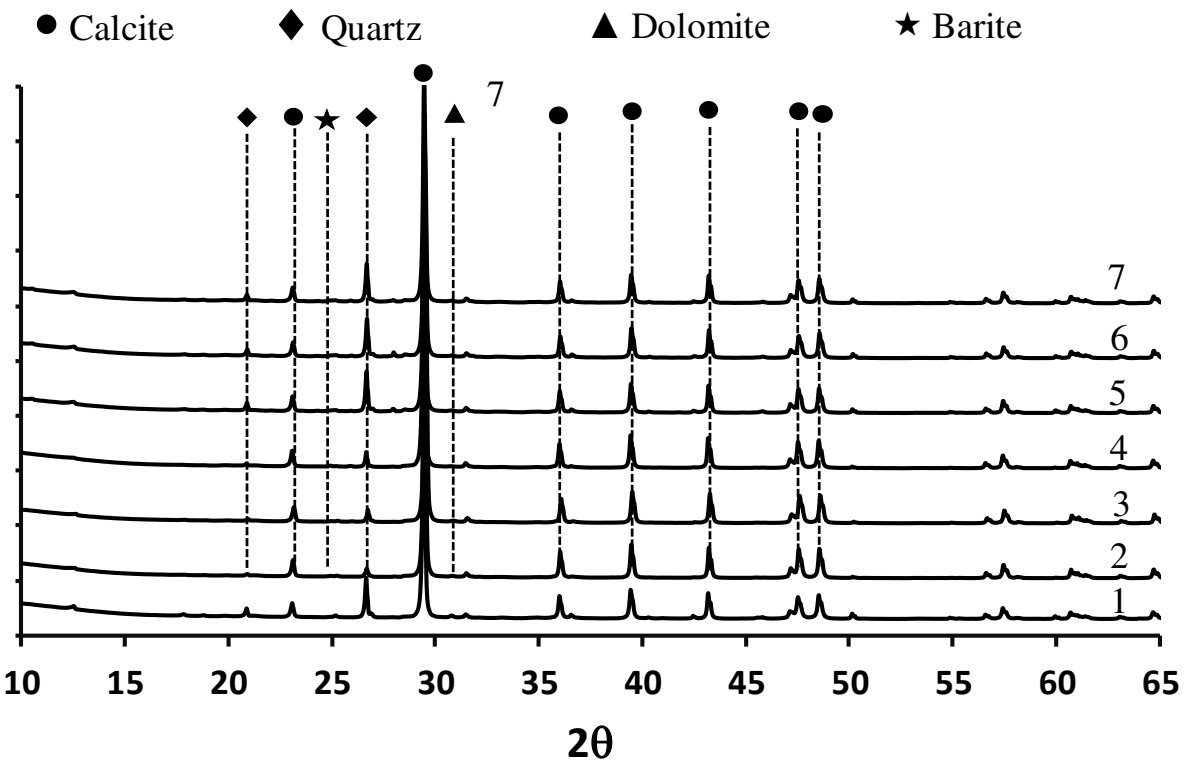

1. RMX_{REF} 2. RMX1 3. RMX2 4. RMX3 5. RMX4 6. RMX5 7. RMX6

Fig. 5. Raw mixes X-ray diffractometry.

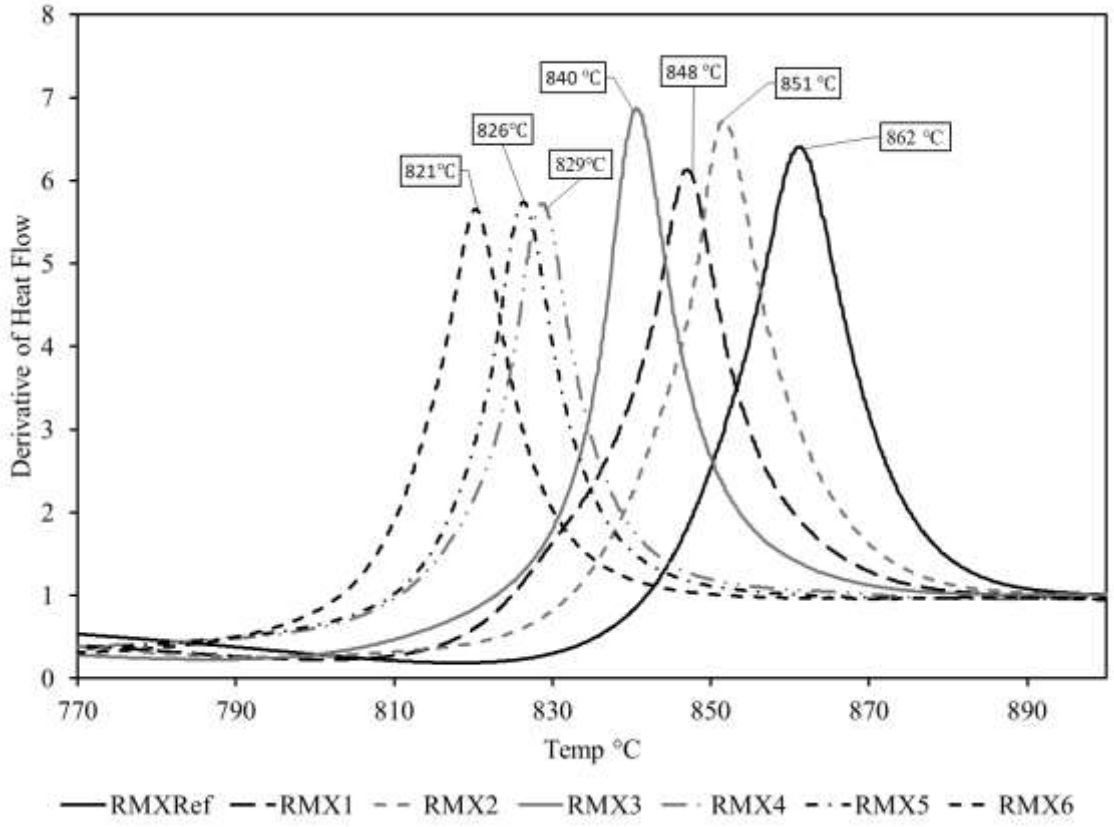

Fig. 6. TG curve on decarbonation of raw mixes.

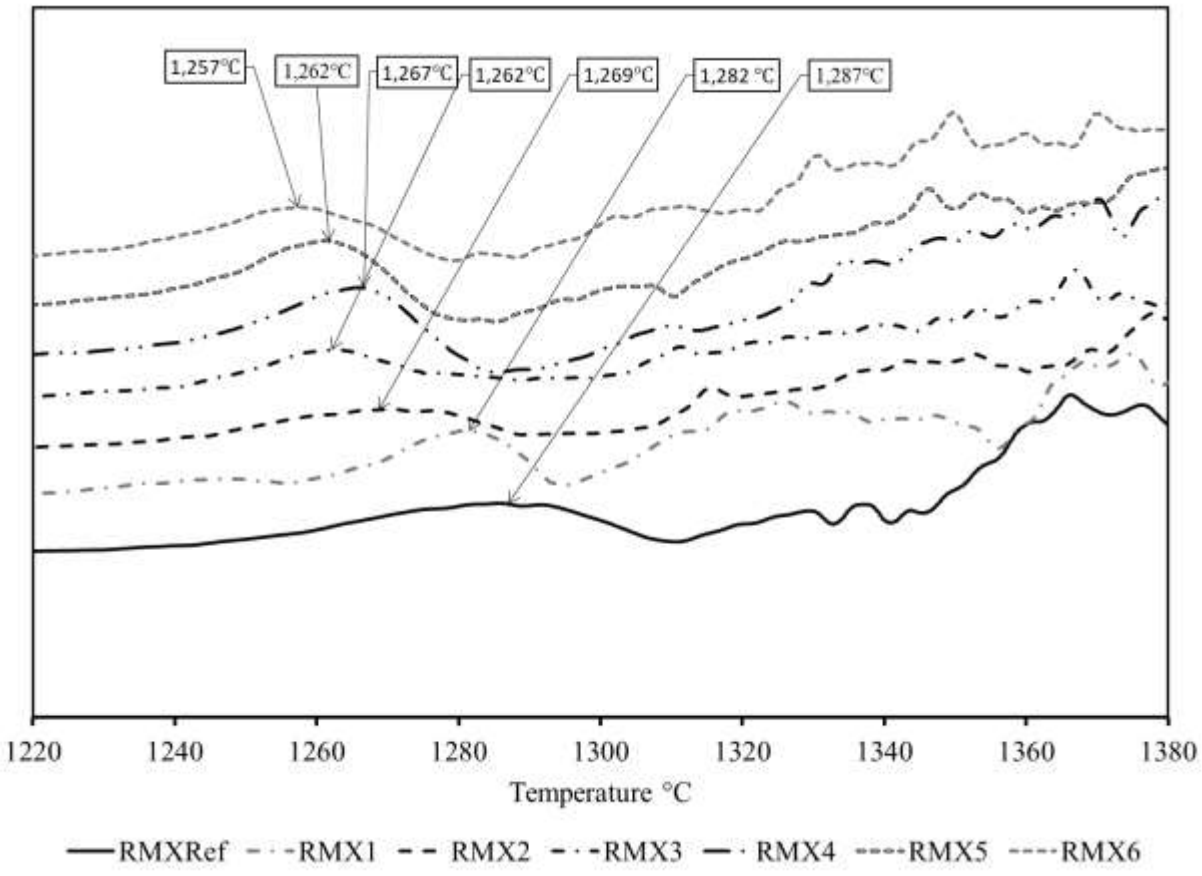

Fig. 7. TG curve - phase formation of raw mixes.

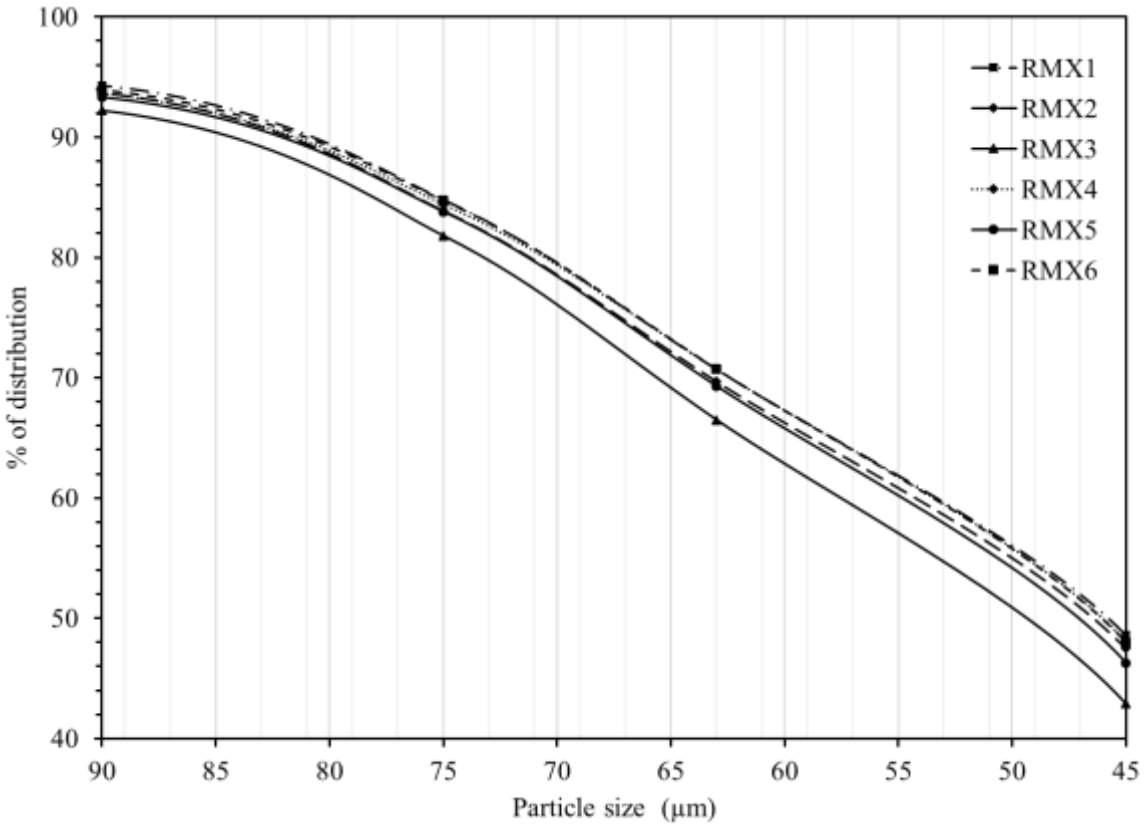

Fig. 8. Particle size distributions of raw mixes.

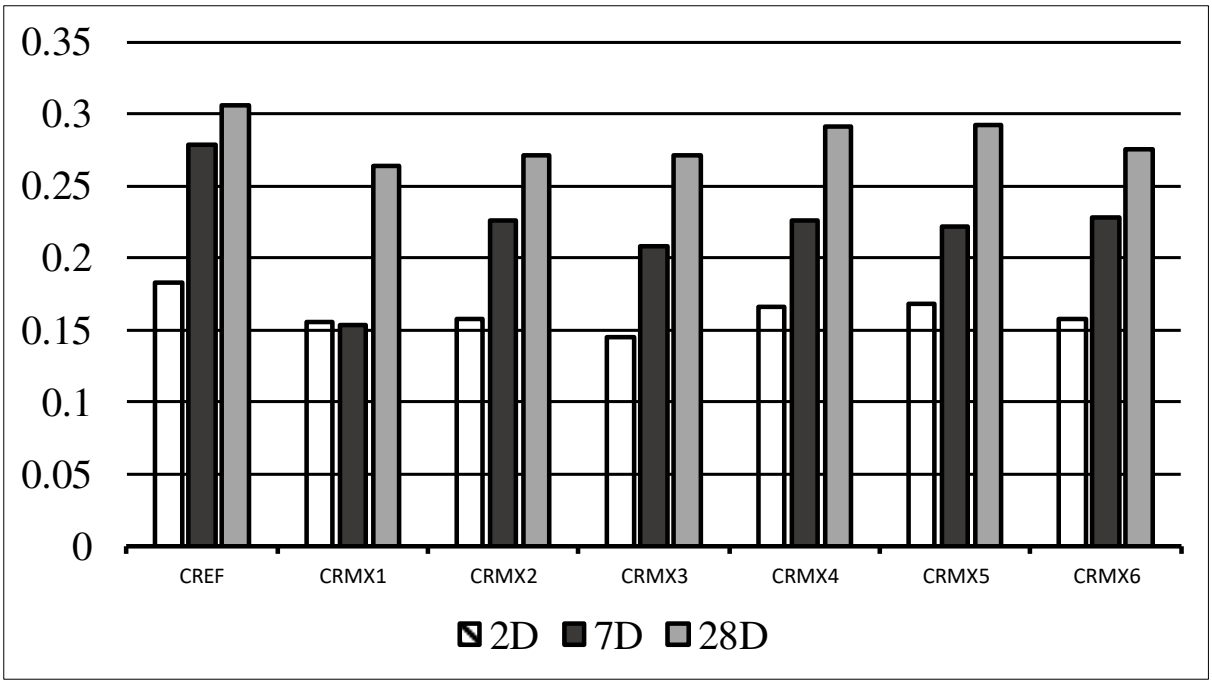

Fig. 9. Cement hydration TG calculation.

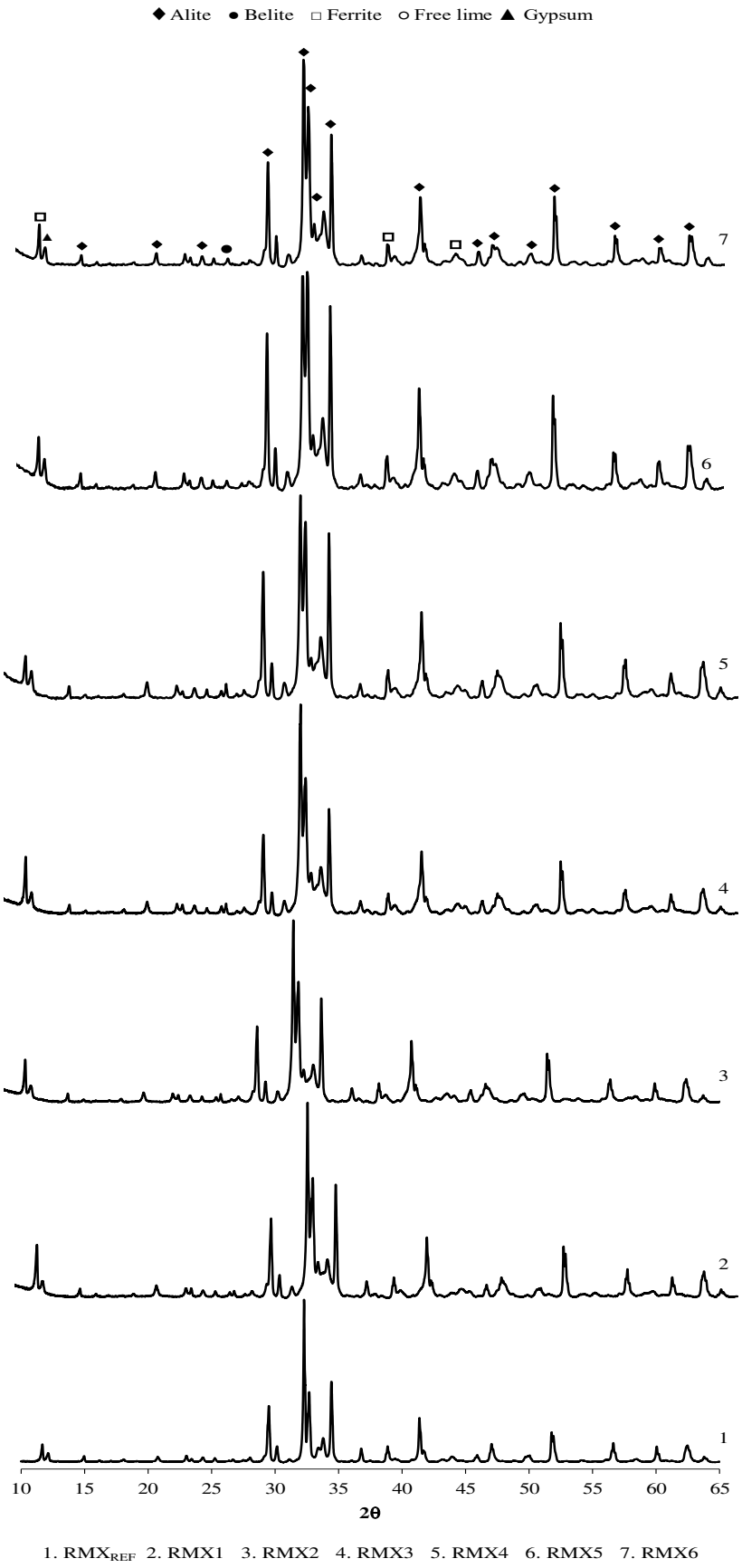

Fig. 10. X-ray diffractometry – cement.